Intra-operative Prostate Motion Tracking Using Surface Markers for Robot-Assisted Laparoscopic Radical Prostatectomy

Mehdi Esteghamatian[a,b*], Kripasindhu Sarkar[b], Stephen E. Pautler[c,d], Elvis C.S. Chen[a], and Terry M. Peters[a,b]

[a]Imaging Research Laboratories, Robarts Research Institute,
[b]Biomedical Engineering Graduate Program, The University of Western Ontario,
[c]Divisions of Urology, Department of Surgery and Division of Surgical Oncology, Department of Oncology, The University of Western Ontario
[d]Canadian Surgical Technologies & Advanced Robotics London, Ontario, Canada.

ABSTRACT

Radical prostatectomy surgery (RP) is the gold standard for treatment of localized prostate cancer (PCa). Recently, emergence of minimally invasive techniques such as Laparoscopic Radical Prostatectomy (LRP) and Robot-Assisted Laparoscopic Radical Prostatectomy (RARP) has improved the outcomes for prostatectomy. However, it remains difficult for the surgeons to make informed decisions regarding resection margins and nerve sparing since the location of the tumor within the organ is not usually visible in a laparoscopic view. While MRI enables visualization of the salient structures and cancer foci, its efficacy in LRP is reduced unless it is fused into a stereoscopic view such that homologous structures overlap. Registration of the MRI image and peri-operative ultrasound image using a tracked probe can potentially be exploited to bring the pre-operative information into alignment with the patient coordinate system during the procedure. While doing so, prostate motion needs to be compensated in real-time to synchronize the stereoscopic view with the pre-operative MRI during the prostatectomy procedure. In this study, a point-based stereoscopic tracking technique is investigated to compensate for rigid prostate motion so that the same motion can be applied to the pre-operative images. This method benefits from stereoscopic tracking of the surface markers implanted over the surface of the prostate phantom. The average target registration error using this approach was 3.25±1.43mm.

Keywords: Robotic-assisted Laparoscopic Radical Prostatectomy, Laparoscopic Surgery, Motion Tracking, Motion Compensation, Image Registration, Image Integration, Enhanced Reality

1. INTRODUCTION

Prostate cancer is the second most common cancer among Western males, with one in 7 developing the disease during his lifetime (the risk is highest after age 60), and one in 28 dying of it. The morbidity rates exist in spite of the fact that PCa is curable at early stages with a survival rate of therapy being over 96%.[1] Radical prostatectomy has traditionally been employed via retropubic or open perineal procedures and more recently by robot-assisted laparoscopy.[2–4] Although the interior of the abdominal cavity is clearly visualized via a stereoscopic laparoscope, the distribution of the malignancy and locations of the cancer foci are subcutaneous; making it difficult to optimize surgical margins to both ensure the effective resection of any extra-capsular tumor expansion, and also to maximize sparing of the neurovascular bundles.

Dynamic Contrast Enhanced (DCE) and T2 weighted MRI have the potential to assist in the diagnosis of cancer in the prostate and image the three dimensional distribution of the tumour.[5] However, the efficacy of such MR imaging to guide the surgeon is reduced unless it is fused with the prostate laparoscopic video as viewed by the surgeon during a laparoscopic prostatectomy procedure .

*Send Correspondence to M.E.: Email: mehdie@imaging.robarts.ca

Medical Imaging 2012: Image-Guided Procedures, Robotic Interventions, and Modeling,
edited by David R. Holmes III, Kenneth H. Wong, Proc. of SPIE Vol. 8316, 83162N
© 2012 SPIE · CCC code: 1605-7422/12/$18 · doi: 10.1117/12.911151

Cohen *et al.*[6] investigated the performance of such an image guided intervention during different stages of a typical prostatectomy procedure, by simply overlaying stationary laparoscopic images with the pre-operatively preprocessed MRI of the target tissue. The authors noted that, based on surgeons' statements, the integrated laparoscopic view is of greatest assistance for nerve sparing and mobilizing the apex of the prostate; however, since the prostate moves due to interaction with the surgical tools and patient motion, compensating for prostate motion during the procedure is an important step to maintain the alignment between the preoperative model and real-time video.

In nephrectomy, Baumhauer *et al.*[7] attempted monocular target pose estimations and navigation methods for laparoscopic partial nephrectomy. Here the authors used a mobile C-Arm and surface markers (surgical aids). However, monocular pose estimation methods are sensitive to noise due to the assumption that the geometry of target tissue is known during the partial nephrectomy procedure.

Ukimura *et al.*[8] proposed optical tracking techniques to fuse 3D TRUS with laparoscopic images whereby infrared optical tracking system was used to perform registration. However, such tracking and fusion is usable only to the point of detachment of the prostate from the rectal wall (which occurs during the process to remove the prostate). In addition, direct line of sight must be maintained for both laparoscope and the ultrasound probe placed between patient's legs.

In this paper, a stereoscopic tracking technique is presented which does not require any special device except for a few surface markers (surgical aids) pinned to the surface of the prostate to track its motion. While it may seem unusual to pierce an organ with pins to secure such a set of markers, it is noted that since the prostate is to be removed immediately, there is no clinical contraindications for this approach. This method was validated in phantoms, using an optical tracking system as gold standard to assess the accuracy of the image-based stereoscopic tracking.

2. MATERIALS AND METHODS

2.1 Camera Calibration

Finding the projective relation between 3D field of view of the laparoscope and pixel coordinate system is the first step in every augmented reality system. During this step intrinsic and extrinsic parameters of the stereo laparoscopic cameras (Intuitive Surgical stereoscopic laparoscope from Olympus connected to a Snell & Wilcox vision cart with a Kudos Plus TBS100 synchronizer) are measured. Zhang *et al.*[9] proposed a flexible calibration technique by imaging a planar checkerboard pattern from arbitrary orientations. A 6 degree-of-freedom (DOF) sensor (NDI Polaris, Waterloo ON Canada) was affixed to the stereoscopic laparoscope and then both stereoscopic laparoscopic cameras were calibrated using the OpenCV[†] library to assess intrinsic and extrinsic properties of each laparoscopic cameras.[9,10‡] Extrinsic parameters, along with the tracking information of the dynamic reference bodies (DRB) were specifically used to measure calibration matrix (the transform from optical origin of the left camera to the 6DOF optical sensor, DRB1, denoted by ${}^{DRB1}T_{CAM}$, see Figure 5). Having the intrinsic properties of each laparoscopic lenses and the calibration matrix, we are able to bring the virtual camera into the alignment with laparoscope's views, to facilitate fusion of the pre-operative MRI with the real view of the laparoscopic camera. Also, we determine the essential matrix of stereoscopic laparoscope using the calibration matrices of two cameras of the stereoscopic laparoscope for the triangulation step.

2.2 Triangulation and Depth Reconstruction

Triangulation is employed in stereoscopic tracking to compute the 3D positions of surface markers given their 2D stereoscopic projections. Each projection provides a ray emanating from the target, and the intersection of the rays passing through the two lenses of the laparoscope determines the 3D location of the object from laparoscope point of view (see Figure 1). However, since there is always image noise and the resolution of the digital images is limited, the accuracy of triangulation is constrained. Therefore, it is important to determine the maximum useful tracking depth.[11] To assess this depth, an optically tracked checkerboard pattern was placed in front of a stereoscopic laparoscope (such as is used with the daVinci Surgical Robot) at different depths in the

[†]http://opencv.willowgarage.com/wiki

[‡]Note that OpenCV uses the method of Brown *et al.*[10] to compensate for lens distortion.

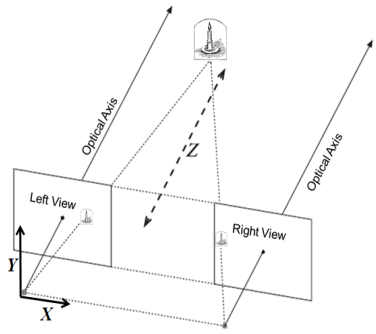

Figure 1. Triangulation using stereoscopic projections.

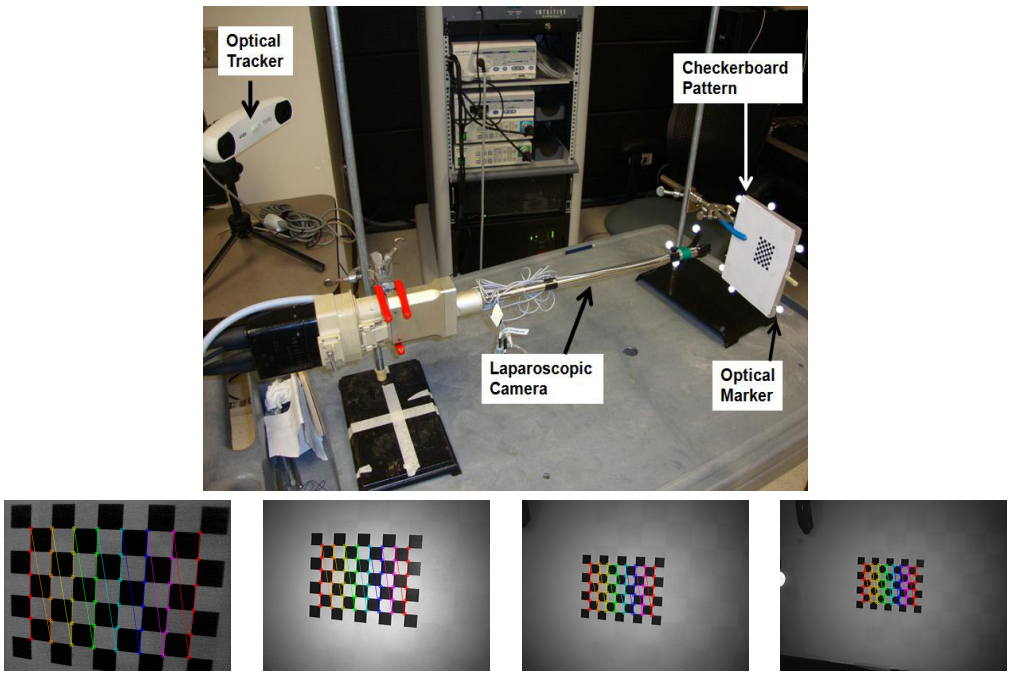

(a) (b) (c) (d)

Figure 2. Experimental configuration for 3D triangulation of the checkerboard corners in different depths (top). Laparoscopic views of the detected checkerboard corners in depths 55, 110, 150, and 185mm from left to right (bottom).

direction of the camera optical axis (viewing axis) (see Figure 2 and Figure 1). Having two 2D stereo images, the 3D positions of the corners (used as corresponding features in the stereoscopic views) were calculated. The measured 3D positions were then compared to the true 3D locations of the corners (measured by the optical tracking system) to assess the triangulation error (see Figure 3).

In practice, rather than attempting to track the position and rotation of the prostate directly from anatomical surface landmarks (which are often poorly defined and suffer from specular reflection artifacts), we instead implant several easily identifiable marker pins into the prostate surface visible to the laparoscopic camera, and use those as the reference marker points.

2.3 Phantom Development

The prostate lies between the pubic bones, constraining rotation and translation of the prostate in a typical LRP to a maximum of approximately 60° and 40mm, respectively according to our surgical co-author. To simulate

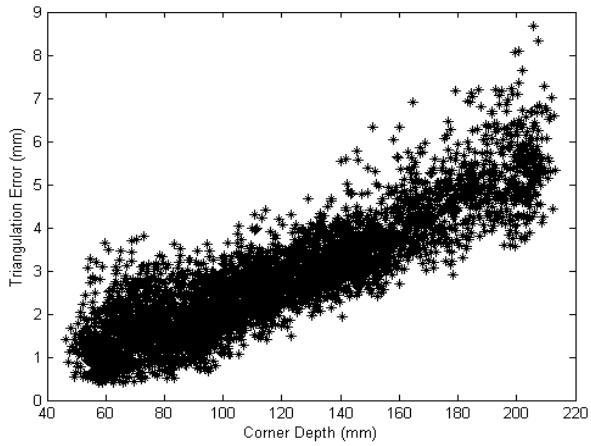

Figure 3. Triangulation error(mm) for corners of checkerboard pattern in different depths using stereoscopic laparoscope. Triangulation error is less than 3.5mm for corners less than 100mm far from optical origin.

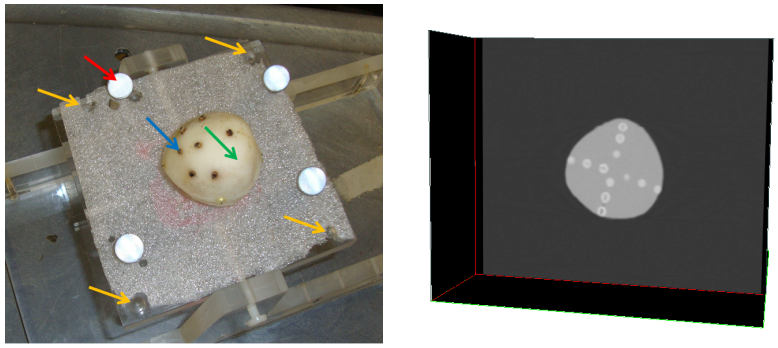

Figure 4. a) Prostate phantom (green arrow), divots (yellow arrows), and passive optical marker (red arrow), surface markers (blue). b) Spherical targets, Teflon® beads implanted inside the phantom as shown in CT.

the prostate gland, we developed a prostate phantom using Poly-Vinyl Alcohol Cryogel (PVA-C) as a tissue-mimicking material.[12] A custom designed mold was used to shape the PVA-C to represent a realistic prostate (see Figure 4). Seven surface markers (wood pins, 1.8mm diameter, 7mm length) were attached to the surface for tracking by the stereoscopic laparoscopic cameras. Also, twelve spherical Teflon® beads were implanted inside the phantom in a cross-shaped format (see Figure 4) for validation and a CT scan (image size 512×512×173, spacing 0.273×0.273×0.625mm) was acquired to represent internal structures that potentially can be provided by a pre-operative 3D DCE or T2 weighted MR image. Infra-red reflective spheres were attached to the phantom frame so that the motion of the phantom could be tracked and the resulting (gold standard) position of the embedded markers determined.

2.4 Alignment Method

One efficient means of tracking prostate motion is to track 3D position of surface markers using triangulation and to apply the resulting transformation to the pre-operative MRI data. The 3D positions of the surface markers are triangulated using left and right 2D laparoscopic images at the beginning of the interventional procedure, and subsequently during the procedure. A point-based tracking brings the current positions of the surface markers into the alignment with the initial positions in order to compensate for the motion of the prostate with respect to its initial position. The same tracked motion can then be applied to MRI-derived pre-operative model to keep the laparoscopic view integrated with pre-operative model.

The triangulation and point based registration computation can be executed at a rate of better than 20Hz, making this method suitable to track motion in real-time. Unlike real-time intensity based registration of

ultrasound images which stops when prostate is not in contact with the rectal wall (due to the air gap between the two tissues), prostate motion can be compensated during the entire procedure using stereoscopic tracking as long as surface markers are in the field of view of laparoscopic cameras.

In the following, we demonstrate such stereoscopic tracking of implanted surface makers to compensate prostate motion during the procedure.

To assess the 3D positions of the surface markers, first the surface markers are identified manually in the left and right stereoscopic images acquired by the laparoscope viewing the base of the prostate phantom. Since the left and right cameras of the laparoscope are calibrated and their intrinsic and extrinsic parameters are known, triangulation can determine the 3D positions of the surface markers with respect to left camera coordinate system. Having the positions of the surface markers, point-based registration determines the position of the prostate relative to camera coordinate system. Let ${}^{CAM}T_{PR}$ denote the corresponding transform defined during triangulation and point based registration step (see Figure 5). Let ${}^{DRB1}T_{CAM}$ denote calibration matrix, the transform from the optical origin for the left lens with respect to the DRB attached to the camera calculated through the calibration process (see Figure 5) and ${}^{OTS}T_{DRB1}$ is the pose of the DRB affixed to laparoscopic camera. The following equation describes the relation between the tracked position of each implanted target (interior cross-shaped spherical implanted targets denoted by $({}^{PR}P)$) in the pre-operative model coordinate system (MRI-derived model coordinate system in clinical practice, but CT coordinate system for this experiment) and their homologous tracked position in the reference frame of optical tracker measured by stereoscopic tracking:

$$ {}^{OTS}P = {}^{OTS}T_{DRB1} \times {}^{DRB1}T_{CAM} \times {}^{CAM}T_{PR} \times {}^{PR}P \tag{1} $$

where, ${}^{OTS}P$ is the corresponding 3D position of the ${}^{PR}P$ in the coordinate system defined by optical tracking system.

2.5 Validation

In the following we assume that the pre-operative image volume (DCE or T2 MRI in clinical practice, or the CT scan of the phantom for the the purpose of this experiment) has been accurately placed relative to the laparoscopic view either via an MR/US registration techniques or via a manual image fusion technique that overlap the pre-operative image volume with the endoscopic view at the appropriate depth and scale.[13,14]

For validation purposes we employed targets simulating tumor, implanted inside the phantom. The ground truth locations are assessed using optical passive markers affixed to the phantom frame. The relative transform from phantom coordinate system to optical tracking sensor (DRB2) (affixed to the phantom frame) coordinate system (${}^{DRB2}T_{PR}$, see Figure 5) is determined by performing a calibration using four divots milled in the phantom frame (see Figure 4). This transform is applied to the known position of the implanted markers in the CT image to determine their position after applying displacements and rotations to the phantom. Also, let ${}^{OTS}T_{DRB2}$ denote the position and orientation of DRB attached to phantom frame (see Figure 5). Having these two transforms, the true locations of the implanted markers are assessed as follows:

$$ {}^{OTS}P^{true} = {}^{OTS}T_{DRB2} \times {}^{DRB2}T_{PR} \times {}^{PR}P \tag{2} $$

where ${}^{OTS}P^{true}$ is the true location of the implanted target in optical tracker coordinate system.

The typical range of translation and rotation of the prostate during prostatectomy procedure is 40mm and 60° degrees according to our surgical co-author. Also, the laparoscopic camera observes an oblique angle with respect to the patient body. Prostate phantom was translated in different directions and rotated around three rotation axes (Anterior-Posterior (AP), Left-Right(LR), and Superior-Inferior(SI), see Figure 6).

Having inferred the tracked positions of implanted targets (${}^{OTS}P$) using the transform computed from the stereoscopic tracking and their gold standard positions derived from optical tracking system (${}^{OTS}P^{true}$), the target registration error (TRE) was calculated using the following equation:

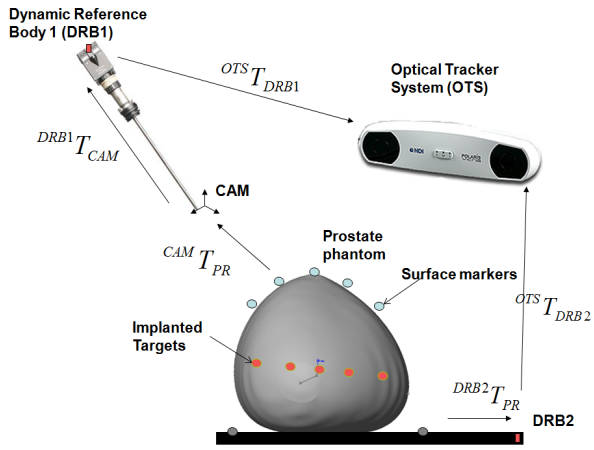

Figure 5. Tracking of the prostate motion using surface markers.

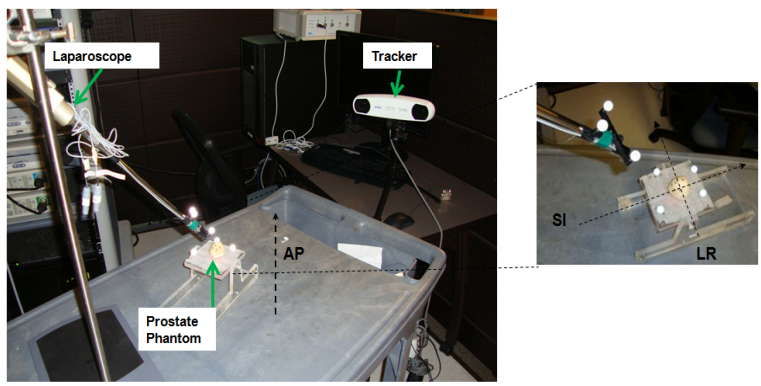

Figure 6. Experiment configuration.

$$TRE = \frac{1}{n}\sum_{i=1}^{n} \| {}^{OTS}P_i^{true} - {}^{OTS}P_i \| \tag{3}$$

where n is the number of targets and $\|.\|$ calculates the magnitude of its argument.

3. RESULTS

Accuracy assessment (see Figure 3) of triangulation in different depths shows that it can assess the 3D position with accuracy better than 3.5mm for corresponding features which are less than 10cm from the lenses of the laparoscope in the direction of the optical axis of camera. This depth corresponds to the typical distance of the tissue from the laparoscopic camera during RARP. At this depth, the prostate phantom was translated from -20mm to 20mm with respect to its initial position in AP, LR, and SI directions as described above. The TRE was reported for different translations represented in Table 1. The phantom was also rotated from -30° to 30° around AP, LR, and SI directions (TRE reported in Table 2 for each rotation angle for every 15°).

4. CONCLUSION

Our tracking method employs triangulation of surface markers to track prostate motion during a RARP so that the registered pre-operative images can follow the same motion to integrate with the laparoscopic view. Triangulation accuracy was assessed at different depths to determine the optimal tracking depth from the laparoscopic camera, where the tracking can perform accurately. The maximum useful tracking distance corresponded to the

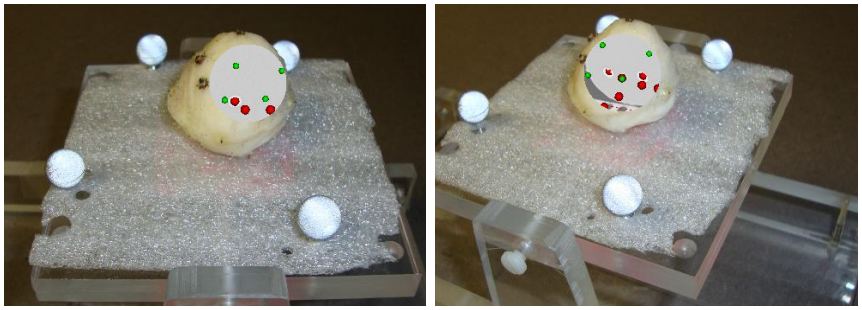

Figure 7. Two representative fused views of the laparoscopic cameras and 3D image volume showing surface markers (green spheres) and implanted targets(red spheres).

Translation(mm)	-20	-10	0	10	20
TRE (mm) in AP	3.24 ± 1.21	2.85 ± 1.32	3.38 ± 0.93	2.97 ± 1.31	3.34 ± 1.11
TRE (mm) in LR	3.44 ± 1.32	3.31 ± 1.35	3.15 ± 1.35	3.33 ± 1.42	3.25 ± 1.41
TRE (mm) in SI	3.25 ± 1.45	3.32 ± 1.13	3.34 ± 1.44	3.15 ± 1.36	3.19 ± 1.38

Table 1. TRE for different amount of translation in AC, LR, and SI directions.

typical laparoscope-organ distance when performing a RARP. The prostate phantom, employed to investigate the accuracy of the tracking, had markers attached to the surface for stereoscopic tracking and also implanted targets simulating tumor for validation purposes. Motion of a prostate typical during the RARP were applied to the phantom. Three-dimensional positions of the surface markers were triangulated by their 2D positions in the left and right images of the stereoscopic laparoscope to assess rotation and translation of the prostate phantom. Measured location of implanted targets were used to assess TRE.

The main advantage of stereoscopic tracking is that it has a closed-form solution,[15] and there is no issues regarding local minima. Stereoscopic tracking is also fast because it makes use of only two projection images of the targeted tissue. Besides, unlike ultrasound based tracking it can continue throughout the prostatectomy procedure even when the prostate is not connected to the rectal wall, as long as homologous markers are in the field of view of the stereoscopic laparoscope. Finally it requires minor modification (application of surface markers) to the conventional robotic clinical procedure compared to other techniques such as optical tracking proposed by Ukimura *et al.*[8] and monocular tracking by Baumhauer *et al.*[7]

The future goal of this project is visualization of the enhanced view of the laparoscope in such a way that homologous features in pre-operative model and laparoscope overlap so that surgeons can see locations of the cancer foci beneath the surface of the tissue, and therefore, they can decide a better margin surrounding the prostate and make informed decisions regarding nerve sparing. Figure 7 illustrates representative fused views of the pre-operative image volume (CT image in this experiment) and laparoscopic views of the phantom.

5. ACKNOWLEDGMENTS

The first author thanks John Moore and Christopher Wedlake for technical support. This project was supported by the Canadian Institutes of Health Research (CIHR) CTP 87515, The Natural Sciences and Engineering Research Council Collaborative Research and Training Experience (CREATE) Program in Computer-Assisted Medical Interventions (CAMI), Canada Foundation for Innovation(CFI), and Cancer Care Ontario (CCO).

Angle(degree)	-30	-15	0	15	30
TRE (mm) in AP	3.12 ± 1.32	3.51 ± 1.32	3.15 ± 1.23	3.21 ± 1.37	3.18 ± 1.21
TRE (mm) in LR	3.17 ± 1.15	3.49 ± 1.27	3.13 ± 1.42	3.39 ± 1.09	3.41 ± 1.12
TRE (mm) in SI	3.38 ± 1.12	3.57 ± 1.34	3.28 ± 1.13	3.31 ± 1.20	2.91 ± 1.17

Table 2. TRE for different rotation angles around AC, LR, and SI directions.

REFERENCES

[1] Newson, E., Gnreux, M., and Ascah, B., "Prostate cancer statistics," *http://www.cancer.ca/* (2011).

[2] Patel, V. R., Jr, M. F. C., and Shah, S., "Robotic assisted laparoscopic radical prostatectomy: a review of the current state of affairs," **61**, 309–314 (Jan 2007).

[3] Smith, J. A. and Jr, S. D. H., "Robotic-Assisted laparoscopic prostatectomy: Do minimally invasive approaches offer significant advantages?," *American Society of Clinical Oncology* **23**(32), 8170–75 (2005).

[4] Appledorn, S. V., Bouchier-Hayes, D., Agarwal, D., and Costello, A. J., "Robotic laparoscopic radical prostatectomy: Setup and procedural techniques after 150 cases," *Urology* **67**, 364–367 (Feb. 2006).

[5] Puech, P., Betrouni, N., Makni, N., Dewalle, A.-S., Villers, A., and Lemaitre, L., "Computer-assisted diagnosis of prostate cancer using DCE-MRI data: design, implementation and preliminary results," *Int J CARS* **4**(1), 1–10 (2008).

[6] Cohen, D., Mayer, E., Chen, D., Anstee, A., Vale, J., Yang, G., Darzi, A., and Edwards, P. E., "Augmented reality image guidance in minimally invasive prostatectomy," *Prostate Cancer Imaging Computer-Aided Diagnosis Prognosis and Intervention* **6367/2010**, 101–110 (2010).

[7] Baumhauer, M., Simpfendrfer, T., Mller-Stich, B. P., Teber, D., Gutt, C. N., Rassweiler, J., Meinzer, H. P., and Wolf, I., "Soft tissue navigation for laparoscopic partial nephrectomy," *Int J CARS* **3**, 307–314 (2008).

[8] Ukimura, O. and Gill, I. S., [*Contemporary Interventional Ultrasonography in Urology*], InTech (2011).

[9] Fix, M. and Zhang, Z., "Flexible camera calibration by viewing a plane from unknown orientations. in: Proceedings of the 7th international conference on computer vision," *Urology* **61**, 612–616 (Mar. 2003).

[10] Brown, D., "Close-range camera calibration," *Photogrammetric Engineering 37* (1971).

[11] Sun, W. and Cooperstock, J. R., "Requirements for camera calibration: Must accuracy come with a high price?," *Application of Computer Vision, 2005. WACV/MOTIONS '05 Volume 1. Seventh IEEE Workshops on* , 356–361 (2005).

[12] Surry, K. J. M., Austin, H. J. B., Fenster, A., and Peters, T. M., "Poly(vinyl alcohol) cryogel phantoms for use in Ultrasound and MR imaging," *Phys In Med & Biol* **49**(24), 5529–46 (2004).

[13] Esteghamatian, M., Pautler, S. E., McKenzie, C. A., and Peters, T. M., "A 2D to 3D ultrasound image registration algorithm for robotically assisted laparoscopic radical prostatectomy," *SPIE Medical Imaging 2011* (7962-70) (2011).

[14] Narayanan, R., Kurhanewicz, J., Shinohara, K., Crawford, E., Simoneau, A., and Suri, J., "MRI-Ultrasound registration for targeted prostate biopsy," *Biomedical Imaging: From Nano to Macro, 2009. ISBI '09. IEEE International Symposium on* , 991–994 (July 2009).

[15] Hartley, R. I. and Sturm, P., "Triangulation," *Computer Vision and Image Understanding* , 146–157 (1997).